Asymmetric Hydrogen Bonding and Orientational Ordering of Water at Hydrophobic and Hydrophilic Surfaces: A Comparison of Water/Vapor, Water/Talc, and Water/Mica Interfaces

Jianwei Wang,*,† Andrey G. Kalinichev,‡ and R. James Kirkpatrick§

Department of Geology and NSF WaterCAMPWS, University of Illinois at Urbana-Champaign, 1301 West Green Street, Urbana, Illinois 61801

Received: February 27, 2009; Revised Manuscript Received: April 21, 2009

Interfaces involving aqueous fluid phases play critical roles in natural and technologically important systems, and the atomic scale differences between interfaces involving hydrophobic and hydrophilic substrates are essential to understanding and manipulating their chemical and physical properties. This paper compares computational molecular dynamics results for the atomic density profiles, H-bonding configurations, and orientational ordering of water molecules at three different and illustrative interfaces. These are the free liquid water surface, which can be considered hydrophobic, and the interfaces of liquid water with talc (001) and muscovite (001) surfaces, which are prototypical hydrophobic and hydrophilic inorganic oxide surfaces, respectively. The results clearly demonstrate the importance of substrate structure and composition in controlling interfacial behavior and illustrate the differences between the vapor interface and those involving solids. The atomic density profiles of water at the solid interfaces show substantial layering, with the details related to the composition and crystal structure of the substrate. In contrast, there is no significant layering at the water−vapor interface. Relative to bulk water, the average density of water at the talc (001) surface is reduced about 9−15% within 6−10 Å from the interface. This is equivalent to a depletion layer about 0.8 Å thick with respect to the similar but hydrophilic mica (001) surface. There is no well-defined vaporlike volume for the talc interface however, and the reduced number of water molecules is spread across the interfacial region. For the free liquid water surface, the results show an asymmetric H-bonding environment and charge density oscillations that provide an additional explanation for the previously observed separation of anions and cations at the surfaces of aqueous solutions. Thus, a delicate imbalance between the accepted and donated H-bonds of interfacial water molecules at this surface, and by inference other hydrophobic and hydrophilic surfaces, determines the preference of charged ions for the interface.

Introduction

The atomic- and molecular-scale structure and dynamics of water are strongly perturbed at interfaces with other materials, and the resulting changes in physical and chemical properties are of significant interest in many environmental, technological, and biological systems.[1−9] Such interfaces can range from strongly hydrophilic to strongly hydrophobic. A free surface of liquid water can be viewed as a hydrophobic liquid−vapor interface, because the interactions between the liquid and vapor phases are weak or nearly absent.[6,10,11] The behavior of this interface is particularly important in many problems in atmospheric science. For instance, in the marine boundary layer, enhanced activity of halide ions at the air/water interface of sea-salt aerosols has strong impact on the chemical composition of the atmosphere.[9,12,13]

Although significant recent progress has been made in understanding the aqueous liquid−vapor interface,[3,6,8,9,14−21] its molecular-scale structure is still not fully understood. In particular, although there are energetic similarities between the liquid−vapor and hydrophobic interfaces, there are also fundamental differences. H_2O molecules at hydrophobic solid surfaces are constrained by so-called "excluded volume" or "hard wall" effects[22,23] due to the geometrical constraints of the finite size of the molecules and molecular packing at the surface. In contrast, H_2O molecules at the free liquid surface are spatially much less constrained by the vapor. Thus, these two kinds of hydrophobic interfaces should result in different molecular-scale structures and local hydrogen bonding arrangements near the interface, leading to their different properties.

We present here the results of molecular dynamics (MD) computer simulations comparing the structure, H-bonding topology, and orientational ordering of H_2O molecules at the free liquid water surface with those at the (001) surfaces of talc and muscovite mica, which are representative of naturally occurring hydrophobic and hydrophilic oxide surfaces, respectively. Our objective is to clarify and quantify the similarities and differences of the atomistic structures between the liquid water−vapor interface and hydrophobic and hydrophilic aqueous interfaces of typical solids with a specific focus on the structure, molecular orientation, and the role of H-bonding. The results show that different local H-bonding environments occur spatially mixed with each other within the planes of the three interfaces, that liquid water at the talc surface (and, by implication, at other oxide-based hydrophobic surfaces) is more structured than at the free liquid surface, and that the molecular orientations and

* To whom correspondence should be addressed.
† Present address: Department of Geological Sciences, University of Michigan, Ann Arbor, Michigan 48109.
‡ Present address: Department of Chemistry, Department of Geological Sciences, Michigan State University, East Lansing, Michigan 48824.
§ Present address: College of Natural Science, Michigan State University, East Lansing, Michigan 48824.

10.1021/jp9018316 CCC: $40.75
Published on Web 05/29/2009

prevailing topologies of interfacial H-bonding networks are appreciably different in the three cases. The known asymmetry of the water−vapor interface is shown to be linked to the differences in the average numbers of donated and accepted H-bonds by H_2O molecules at different distances from the surface. The results provide insight into recent experimental sum-frequency vibrational spectroscopy of the liquid−vapor interface and hydrophobic organic interfaces with water[15,18,24,25] and near-edge X-ray absorption fine-structure spectroscopy of liquid water surface.[26]

The structure of bulk liquid water is statically and dynamically disordered, and its investigation remains of substantial current interest.[9,20,21,27−36] A quantitative understanding of the structure and dynamics of the free surface of liquid water is even more challenging, because static and dynamic disordering and fluctuation at the molecular scale impose difficulties in interpretation of experimental results. Molecular modeling has contributed significantly to better understanding and interpretation of the observed phenomena.[6,9,14,19,20,36−39] Previous MD simulations of the liquid−vapor interface have suggested that the water density decreases from its bulk liquid value to zero over a depth of about 7 Å.[14] The results of SFG spectroscopic experiments[15,18] and ab initio MD simulations[19] of the liquid−vapor interface suggest the presence of free (i.e., not H-bonded) OH-groups of water molecules and single-donor and acceptor-only H_2O molecules in the near surface region. The free surfaces of aqueous Na halide solutions also appear to be asymmetrical with the halide ions (especially the larger ones) being concentrated closer to the surface than Na^+.[12,40] Theoretical considerations[6,10,41,42] and experiments[43−48] show that the water density at solid hydrophobic surfaces is lower than in the bulk liquid. Our simulations are consistent with these previous molecular modeling and experimental results and provide further details of the molecular-scale structure of interfacial water and its asymmetric nature: imbalanced H-bonding across the interface at hydrophobic and hydrophilic surfaces.

Talc (001) is a relatively simple but representative natural surface that energetically is clearly hydrophobic with the increasing surface hydration energy per water molecule as the number of surface water molecules decreases.[49] The experimental advancing and receding contact angles for talc (001) surface are 60 and 50°, respectively,[50] also indicating significant hydrophobicity. However, this surface consists of Si−O−Si siloxane linkages that are common for many silicates and can potentially serve as weak H-bond acceptors. Weak H-bond donation from the internal Mg−OH sites is also at this surface. The H_2O molecules at the talc−water interface show a high degree of positional ordering parallel to the surface, reflecting the structure of the underlying substrate.[49]

The (001) surface of muscovite mica contains similar Si−O−(Si,Al) siloxane linkages but with positively charged ions (e.g., K^+) located at the six-member ring cavity surface sites to balance the net negative structural charge due to partial tetrahedral Al^{3+} for Si^{4+} substitution. The result is a hydrophilic surface with the hydration energy per water molecule decreasing as the number of surface water molecules decreases.[51] As for talc, the H_2O molecules at muscovite−water surface show a high degree of positional ordering parallel to the surface.

Methods

Structural Models and MD Simulations. The structure of talc, $Mg_3Si_4O_{10}(OH)_2$, consists of so-called TOT layer (an octahedral layer of $[MgO_4(OH)_2]$ sandwiched between two tetrahedral layers of $[SiO_4]$) stacked along the crystallographic Z direction.[54] All tetrahedral sites are occupied by Si forming $[SiO_4]$ structural units, and all octahedral sites are occupied by Mg forming $[MgO_4(OH)_2]$ units. The TOT layers are thus electrostatically neutral and interact with each other only by weak by van der Waals forces, reflecting the hydrophobic nature of the basal siloxane Si−O−Si (001) surface. The structure of muscovite mica, $KAl_2(Si_3Al)O_{10}(OH)_2$, consists of similar TOT layers composed of two tetrahedral Si/Al sheets that are connected by an Al dioctahedral layer. Some of the Si^{4+} cations in the tetrahedral sites of muscovite are isomorphically substituted by Al^{3+} (Al/Si ratio = 1:3), resulting in a permanent negative structural charge. The layered structure is held together by the presence of charge-balancing interlayer K^+ ions.[55] In our MD modeling, the interatomic interactions within the crystal structures are described by the *CLAYFF* force field,[56] which has been successfully applied to simulate a wide range of minerals and interfaces.[49,51,56−65] The details of the models and the performance of the *CLAYFF* force field for talc and muscovite are described in our previous publications.[49,51−53] For H_2O, we use a flexible version[66] of the simple point charge (SPC) potential. Like other versions of the original SPC potential,[67] this water model reproduces quite well the properties of bulk liquid water.[68] It is compatible with the *CLAYFF* and has already been well tested in a range of aqueous interfacial systems.[49,51,58−65,69] Therefore, we expect the results reported here to be a realistic qualitative characterization of the interactions between water and the surfaces. Quantitatively, however, the results should be expected to be somewhat model-dependent and may vary from one H_2O model to another, since the quantum and many-body effects of water−water and water−surface interactions are incorporated into most of the existing models only effectively and indirectly.

All MD simulations described here were performed at ambient conditions in the *NVT* (constant volume and temperature T = 300 K) ensemble (after a pre-equilibration in the *NPT* ensemble at T = 300 K and P = 0.1 MPa) using standard MD algorithms.[70] The talc and muscovite surfaces were constructed by cleaving the bulk crystal structure parallel to the (001) plane in the middle of the interlayers. The complete interfacial MD simulation cells consist of a substrate (001) talc or mica slab about 20 Å thick (two TOT layers), and a layer of liquid water about 30 Å thick placed in contact with them. The water was pre-equilibrated at 300 K and 0.1 MPa. Periodic boundary conditions were applied to the resulting system in all three dimensions. To create an independent liquid−vapor interface and to minimize the effects of the imposed periodic boundary conditions, the Z-dimension of the simulation supercell was set to 100 Å, resulting in a separation of ~50 Å between the water−vapor interface of water adsorbed on one side of the talc or muscovite slab, and the other (bare) surface. The final X-, Y-, and Z-dimensions of the supercells were 21.14 Å × 18.32 Å × 100 Å for the talc−water system and 17.79 Å × 20.73 Å × 100 Å for the muscovite−water system. The MD time step was 1.0 fs, and the total system was allowed to equilibrate for 500 ps of MD before an equilibrium MD trajectory for each model was accumulated at 10 fs intervals during an additional 500 ps of MD simulation. The details of the MD simulation procedures and parameter settings for mineral−water systems are described in previous publications.[49,51,58,62,63,71]

Similar MD simulations under the same conditions were also performed at hydrophilic (001) surfaces of brucite, $Mg(OH)_2$, gibbsite, $Al(OH)_3$, and hydrotalcite, $Mg_2Al(OH)_6Cl\cdot 2H_2O$.[49] Although the structures of the water−solid interfaces are

significantly different for these systems, the results for the liquid−vapor interfaces are essentially identical and independent of the hydrophilicity or hydrophobicity of the substrates. Thus, only the results for the liquid−vapor surface from the simulations of the muscovite−water system are shown and discussed here.

Analysis of the MD Results. The interfacial water structure was analyzed in terms of the O_{H_2O} and H_{H_2O} atomic density profiles, the distributions of H_2O molecular orientations, and the distributions of interfacial H_2O molecules having a given number of H-bonds as functions of distance from the surface. The computed molecular density profiles, molecular orientation profiles, and H-bond distribution profiles provide an integrated and comprehensive picture of the structural similarities and differences among the water−vapor interface, the water−talc interface, and the water−muscovite interface and can serve as a basis for understanding and predicting experimental results for them. These values were all calculated by averaging over the last 500 ps of the equilibrium MD simulation trajectory.

The cumulative average density of interfacial water is calculated as the molecular density averaged over a volume within a specified distance, d, from the surface. This can be calculated from O_{H_2O} atomic density profile as

$$\rho_{ac}(z) = \int_{-\infty}^{d} \rho(z)dV / \int_{d_0}^{d} dV \quad (1)$$

where $\rho_{ac}(z)$ is cumulative average density, $\rho(z)$ is the O_{H_2O} atomic density profile, d_0 is the starting surface position from which the density is averaged, and dV means the integral volume over the specified region. Therefore, $\rho_{ac}(z)$ is a measure of average water density at the interface within a distance d from the surface.

The molecular H_2O orientation parameters, φ_D and φ_{HH}, are defined for each water molecule by the angles between the surface normal direction and, respectively, the dipole vector ($\mathbf{v}_D$) of the molecule (positive direction from the oxygen end to the hydrogen end of the molecule) and the H−H vector ($\mathbf{v}_{HH}$) from one hydrogen atom to the other. The positive direction of the surface normal is defined from the interface into the liquid. The criteria applied to define the existence of a hydrogen bond are those frequently used in the analysis of bulk liquid water structure: intermolecular O···H distances less than 2.45 Å and angles, β, between the O···O and O−H vectors less than 30°.[72] The threshold distance of $R_{O\cdots H} \leq 2.45$ Å is used because it corresponds to the first minimum of the O···H radial distribution function for the SPC water model under ambient conditions, while the threshold angle $\beta \leq 30°$ is chosen, because it includes 90% of the angular distribution of H-bonds in bulk liquid water under the same conditions.[72,73] For the purpose of H-bond calculations, the oxygen atoms of the talc and mica surfaces are treated in the same way as O_{H_2O} (as potential H-bond acceptors).

Charge density profiles of interfacial water are calculated for each interface based on the O_{H_2O} and H_{H_2O} density profiles. The SPC partial charges are used in the calculations, $+0.41|e|$ for the H atom and $-0.82|e|$ for the O atom.[67]

The Gibbs dividing surface is used as the reference position of the three interfaces ($Z = 0$), as suggested in the literature.[74,75] This dividing surface is defined as the position $Z = 0$ at which the atomic density integral of O_{H_2O} over the volume on the one side of the interface ($Z \leq 0$) equals the deficit with respect to the bulk of the O_{H_2O} atomic density integral on the other, liquid side of the interface ($Z \geq 0$). This position can be easily calculated iteratively from eq 2 using the O_{H_2O} atomic density profile at the interface

$$\int_{-\infty}^{z} \rho(z)dV = \int_{z}^{+\infty} [\rho_0 - \rho(z)]dV \quad (2)$$

Here $\rho(z)$ is the molecular density profile (represented by O_{H_2O}), ρ_0 is the bulk density of liquid water, and dV means the integral is taken over the specified volume. The solution of eq 2 uniquely defines the position of the dividing surface, $Z = 0$. Note that this position does not necessarily coincide with the position d_0 introduced earlier in the eq 1, where d is the distance from the surface, and the surface reference is defined by the average position of the surface bridging O atoms (O_b) for talc and muscovite. This distinction is necessary because the distances between O_b and the Gibbs dividing surfaces are different for these two surfaces.

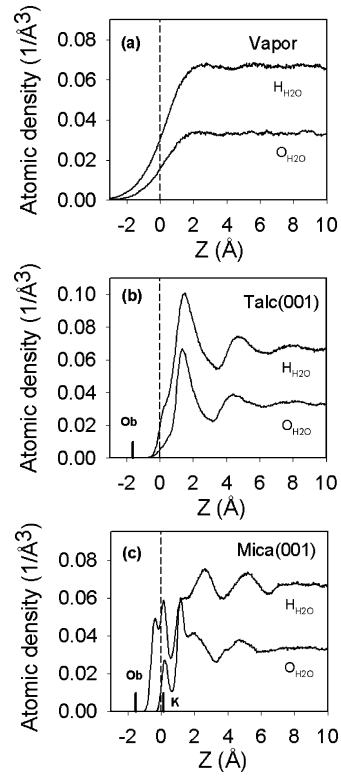

Figure 1. Atomic density profiles of water at (a) water−vapor, (b) talc (001), (c) mica (001). Solid lines are O_{H_2O} and H_{H_2O} densities. $Z = 0$ is defined as the position at the Gibbs dividing surface, indicated as dashed vertical line. The positive direction and surface normal are defined from interface to liquid phase for all figures. Short thick vertical bars indicate the average position of surface bridging oxygens.

Results and Discussion

Atomic Density Profiles. The computed O_{H_2O} and H_{H_2O} density profiles at the free water surface (Figure 1a) show deviations from the bulk liquid density values over about 7 Å across the interface. There is a small, broad maximum at $Z \sim 2.2$ Å for O_{H_2O} and at $Z \sim 2.6$ Å for H_{H_2O}, and the densities then decrease monotonically to zero with decreasing Z, in agreement with previous work.[14,19,76] The O_{H_2O} and H_{H_2O} densities at the maxima are, respectively, ~3 and ~2% higher than the isotropic bulk liquid water density. The most distant water molecules at the water−vapor interface occur at $Z \sim -3.6$ Å. The saturated water vapor density under ambient conditions is 2.559 ×

10^{-5} g/cm^3,[77] and thus in our simulations we expect on average only about 2×10^{-2} H_2O molecules to be entirely in the vapor phase at any time. None were detected during the simulations.

At the talc (001) surface, the O_{H_2O} density increases relatively sharply across the interface to a maximum of about twice the bulk liquid density at $Z \sim 1.3$ Å from the Gibbs dividing surface and then oscillates with a periodicity of about 3.1 Å and progressively smaller amplitude to about 14 Å from the surface (Figure 1b). The H_{H_2O} density also increases rapidly across the interface and shows a shoulder near $Z \sim 0$ Å and a maximum of about 1.5 times the bulk density at $Z \sim 1.5$ Å. Further from the surface, it also oscillates with a periodicity of about 3.1 Å with progressively smaller amplitude to about 12 Å from the surface. Both profiles show a much more pronounced layering of H_2O molecules than at the free liquid water surface. They are, however, quite similar to those of water at planar, not atomistically structured, hydrophobic surfaces, which show pronounced layering with a decaying periodicity of about 3 Å.[41,78,79]

At the muscovite (001) surface, the O_{H_2O} density profile exhibits five distinct peaks at about $Z = 0.3$, 1.0, 2.0, 3.7, and 4.7 Å, and a broad, asymmetric peak around 8.0 Å. The H_{H_2O} density profile also exhibits five distinct peaks but at slightly different locations with $Z = -0.5$, 0.3, 1.0, 3.0, and 5.1 Å, and a broad, asymmetric peak around 7.0 Å. Because electrostatic interactions and H-bonding between H_2O molecules and the surface play significant roles at this interface,[51,80−82] the density profiles (Figure 1c) are much more complex than those at hydrophobic interfaces (Figure 1b). In general, many similarities and differences of water density profiles at various mineral−water interfaces are due to the specific details of the atomic structure of the particular surfaces.[49] Thus, in terms of the peak positions, relative intensities, and peak shapes, the first, second, and fourth peaks at the mica (001) surface are similar to the first three peaks of the water density profile at silica surface with low surface density of hydroxyls,[83] possibly because the two surface lattice structures are similar by having surface O with O−Si−O bonds. On the other hand, at the nonhydroxylated rutile (110) surface, the water O density profile also shows three distinct peaks,[84] but the peaks relative intensities and locations are incompatible with those at the muscovite (001) and silica surfaces.

The talc (001) surface is structurally similar to that of muscovite (001). However, due to the absence of surface charge it is hydrophobic, and the distinct peaks of the water density profiles at the muscovite surface (Figure 1c) become broader and asymmetric at the talc surface (Figure 1b). For instance, for O_{H_2O} the peak at 0.3 Å at muscovite surface corresponds to the shoulder around 0.2 Å at talc surface; the peaks at 1.0 and 2.0 Å at muscovite (001) correspond to the broader and asymmetric peak around 1.3 Å at talc (001); and the peaks at 3.7 and 4.7 Å at muscovite surface correspond to the broader peak around 4.3 Å at talc surface.

The periodic spacing of the density maxima near the talc surface and ideally flat and unstructured hydrophobic surfaces reflect the dominance of steric "excluded volume" effects.[22,23] These effects are geometrical in origin and reflect the layered packing of molecules at any "hard" surface due to the finite size of the molecules. The excluded volume effects are dominant in relatively simple cases of fluid structuring near solid surfaces, such as a hard sphere fluid at a hard wall or a Lennard-Jones fluid at a Lennard-Jones surface.[22] Such hypothetical surfaces are not usually assumed to have specific sites for interaction with water molecules, such as H-bond acceptor and/or donor sites. Because they do not interact strongly with water molecules, they are hydrophobic. Similar equal spacings are observed for density profiles of water at the liquid mercury surface, where the O_{H_2O} density maxima are also about 3 Å apart.[85,86] For water at hydrophobic graphite surface, the O_{H_2O} density profile is quite similar to that at the talc (001) surface in terms of peaks shape and the distance from the surface because of the hydrophobic nature of both surfaces.[53,83,87−90] However, the small shoulder at $Z = 0$ Å (Figure 1b) at the talc surface is not present at graphite surface. This is because the graphite surface lacks the large vacant sites that are present at talc (001) surface, where water molecules can be weakly adsorbed.[49,53]

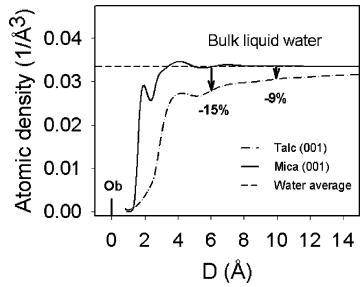

Figure 2. Cumulative average water density as a function of distance from the surface at talc (001). The horizontal dashed line is the bulk liquid water density (0.03345 Å^{-3}); the short vertical bar indicates the averaged position of the surface bridging oxygens (O_b). The solid line is the cumulative average density for water at mica (001) surface by assuming no water density reduction at the surface. The dotted-dashed line is the cumulative average density for water at talc (001) surface with respect to that at mica (001) surface. The zero position here is defined for both surfaces as the average Z-coordinate of the surface bridging oxygens.

The minor deviations from perfect density maxima periodicity at the water−talc interface, including the shoulders and asymmetrical peak shapes, are related to the atomic scale structural details of the talc surface, which do not exist at perfectly flat "hard wall" surfaces often considered in theory. For instance, H_2O molecules can occupy the vacancies in the six-member siloxane rings on the talc surface, giving rise to the small increase of the O_{H_2O} density near 0.3 Å. Similarly, H_2O molecules can donate weak H-bonds to the O_b atoms of the siloxane groups at the talc surface, giving rise to the noticeable shoulder at about 0 Å in the H_{H_2O} density profile (Figure 1b). Such features cannot occur at other relatively smooth hard wall surfaces.[53,83,87−90]

Cumulative Average Water Density near Talc (001)−Water Interface. Theoretical investigations and experimental measurements[42−44,46,91,92] show significant reduction of water density at the free liquid surface and at hydrophobic surfaces. However, experimental determination of the depletion layer thickness contributing to the interfacial density reduction has difficulty at soft hydrophobic surfaces.[46,93,94] For instance, in synchrotron X-ray reflectivity experiments, problems may arise from soft hydrophobic hydrocarbon chains at the surface penetrating into the liquid water phase. Solid hydrophobic surfaces, such as talc (001), have certain advantages in this respect. Our MD simulation results for the water−talc (001) surface show a significant reduction in water density at the interface, consistent with previous experimental and theoretical studies.[42−44,46,92]

The cumulative average density of water oxygen as a function of distance from the surface shows a much greater effect of the density reduction for talc (001) than for muscovite (001) (Figure 2). Assuming neither excess nor depletion of water density at

the hydrophilic muscovite (001) surface, the results yield a reduction of water density at talc (001) equivalent to a 0.79 Å thick depletion layer. This is a reduction of about 15 and 9% at distances of about 6 and 10 Å, respectively, from the surface bridging oxygen positions (O_b), as shown in Figure 2. For this calculation. we count surface K^+ ions as H_2O molecules because of their similar size.[95] The estimated value for the depletion layer thickness is in accord with recent Monte Carlo simulations that suggest values of about 0.6−0.9 Å for a hydrophobic surface with a contact angle between 50°−60°, that is, comparable to talc (001).[42] For hydrophobic surfaces with higher contact angles, the depletion layer thickness increases to a few angstroms.[42,46] The reduction of water density at the talc (001) surface is also qualitatively consistent with recent neutron[44] and X-ray reflectivity measurements[43] that show a 10−15% decrease of water density extended 40 Å into the water phase on a hydrophobic self-assembled monolayer of methoxytri(ethylene glycol) terminated undecylthiolate, and a ∼10% decrease of water density within 15 Å at a hydrophobic paraffin surface. Our MD simulations do not show a distinct vapor layer, void, or vacuum space at the interface, but a gradual reduction in water density over 15 Å next to the surface (Figure 2).

Orientational Ordering of Interfacial Water Molecules. The preferred H_2O orientations at the water−vapor interface are quite different at the three interfaces, reflecting the differences in H-bond donation and acceptance topology, as shown by the computed dipole orientational distributions (Figure 3). At the hydrophobic talc−water and vapor−water interfaces, the molecular orientations are similar in the regions with maximum water density, but quite different in the regions of reduced molecular density. In the regions of maximum molecular densities ($Z \sim 2.2$ Å for the vapor−water interface and ∼1.3 Å for the talc−water interface), the mean H_2O orientation is characterized by $\varphi_D = 90°$ (dipole parallel to the surface; Figure 3 (top, middle)) and $\varphi_{HH} = 90°$ (H−H vector parallel to the surface, data not shown). Thus, the H−O−H molecular plane lies on average parallel to the surface, although the distribution is broad and the peak is less pronounced for the water−vapor interface. This result is in agreement with previous MD simulation results of water at a model molecular hydrophobic surface.[96] In contrast, in the region of lower water density at $Z < 0$ Å for the vapor interface, the orientational distributions have maxima at $\varphi_D \sim 105°$ (Figure 3 (top)) and $\varphi_{HH} \sim 0°$. This orientation indicates that the H−O−H plane is, on average, perpendicular to the surface and that the dipole is pointing away from the liquid phase to the vapor phase at an angle of 15° to the surface. Previous MD simulations of the water−vapor interface[6,14,76] have shown similar H_2O molecular orientations at the surface and also a comparable net dipole orientation. Similar asymmetric orientations of H_2O molecules found at the water−vapor interface (parallel to the surface on the liquid side of the interface and perpendicular to it on the vapor side) were also observed at the water/1,2-dichloroethane liquid−liquid interface,[97] where water molecules can penetrate into the hydrophobic 1,2-dichloroethane phase. In contrast, in the low density near surface region ($Z < 1$ Å) of the talc (001) interface the H_2O dipoles point predominantly toward the liquid phase with $\varphi_D \sim 30°$ (Figure 3 (middle)) and $\varphi_{HH} \sim 90°$. This orientation indicates that the H−O−H plane makes, on average, an angle of about 60° with the surface and that the H_2O dipole is pointing to the liquid phase. This result is consistent with previous Monte Carlo simulations.[98] This orientation is also indicated by the H_{H_2O} atomic density profile (Figure 1b), which shows a shoulder of H-density at $Z < 1$ Å that is more pronounced than that of O_{H_2O}. At the water−mica interface at $Z < 1$ Å (Figure 3 (bottom)), the H_2O dipole is pointing away from the liquid phase ($\varphi_D \sim 150°$), because the water molecules donate hydrogen bonds to the surface oxygens (O_b). This orientation reflects the hydrophilic nature of the surface, where the surface bridging oxygens are the strong interaction sites, as previously suggested.[51]

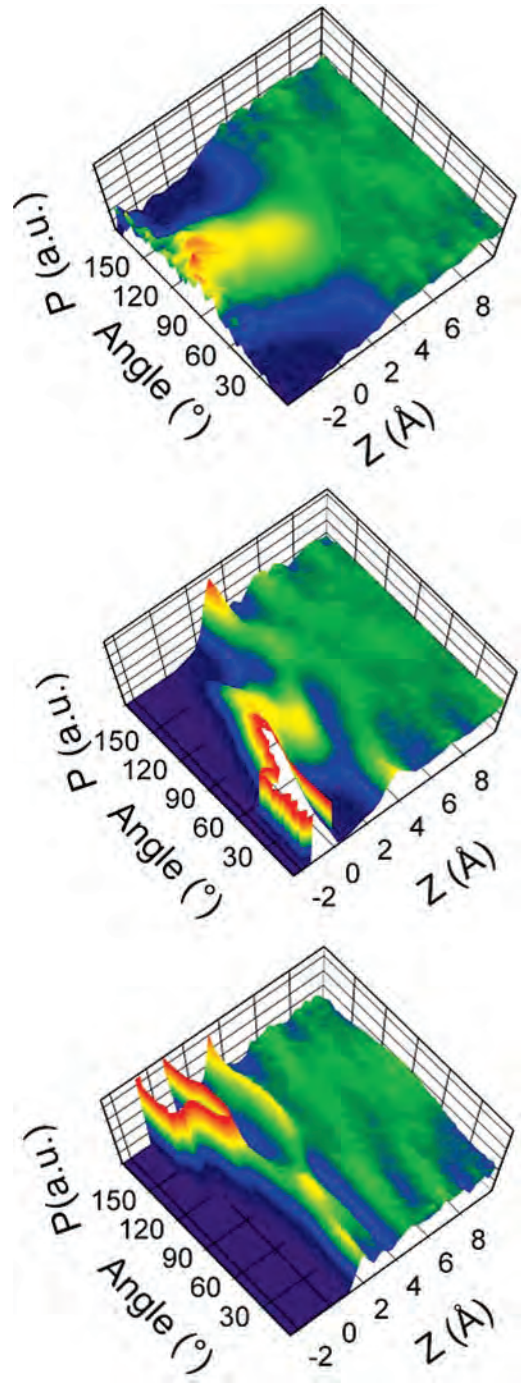

Figure 3. Orientation distribution of water molecules as a function of their distance from the surface. (top) Dipole orientation at liquid−vapor interface; (middle) dipole orientation at talc (001) surface; and (bottom) dipole orientation at mica (001) surface. The probability is normalized by atomic density at given distance and by a sinusoidal function to correct the angular distribution of a vector in space. Color scheme: blue has lower probability and red higher probability.

Asymmetric Topology of Interfacial H-Bonding Networks. The differences in the water structure at the free liquid, talc, and mica surfaces are clearly reflected in different statistics of

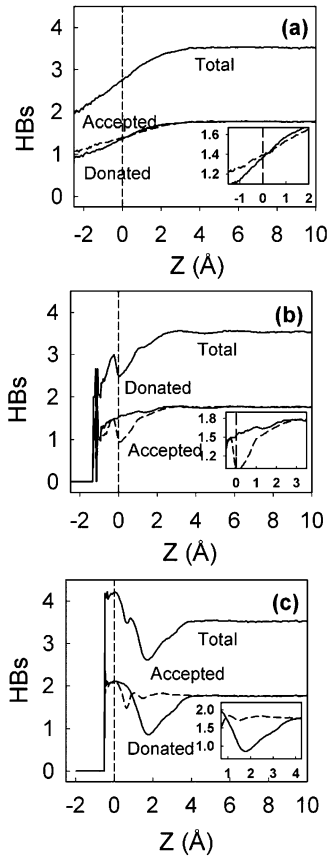

Figure 4. Average number of hydrogen bonds and their donor/acceptor components. (a) Water at liquid−vapor interface; (b) water at talc (001) surface; (c) water at mica (001) surface. Solid lines are total number of H-bonds and average number of donated H-bonds. Dashed lines are accepted H-bonds. Inserts highlight the regions where accepted and donated H-bonds are in imbalance. Vertical dashed lines are the Gibbs dividing surface.

H-bonding accepting/donating configurations (Figure 4). In bulk liquid water, an average H_2O molecule has about 3.2 H-bonds in MD simulations using the SPC potential and our criteria, consistent with previous computer simulations using similar models and H-bonding criteria.[72,99−101] Here, such bulklike behavior occurs at $Z > 10$ Å for the three interfaces (Figure 4), and only small variations around the bulk value occur at intermediate distances of $10 > Z > 4$ Å. For the free liquid water surface, the total number of donated and accepted H-bonds per molecule decreases monotonically to about 2.0 at $Z < -2$ Å (Figure 4a), where the molecular density is significantly reduced (Figure 1a). Similarly, for the talc−water surface, this value also decreases to about 2.0 at $Z = -1$ Å. The reduction in the total number of H-bonds near both surfaces clearly reflects their hydrophobic nature.[11] For the mica−water interface, however, the total number of H-bonds near the surface is about 4, reflecting the hydrophilic character of the surface. The reduction of the total number of H-bonds at $Z = 2$ Å for mica is due to the presence of surface K^+ ions that cannot contribute H-bonds in the region. These results reflect the importance of the hydrogen bonding network of the water molecules in determining the properties of the interface. On average, a lower degree of interfacial H-bonding for water molecules indicates a weaker interaction with the surface, which is characteristic of a hydrophobic surface. This view is also suggested in a recent MD study of water interaction with silica surface, where the properties of the second molecular layer are determined by the water−water hydrogen bonds formed with the water molecules in the first layer.[83]

In bulk liquid water, each molecule has equal probability of accepting and donating H-bonds, but near a surface this is not true. In liquid water, the dynamically averaged balance of accepted and donated H-bonds maintains an approximate isotropy and electrostatic neutrality around each individual H_2O molecule, but at interfaces this isotropic symmetry does not hold.[6,10,78] This asymmetry may be the origin of many unique properties of the free surface of water, including the differences in the behavior of excess anions and cations observed experimentally and computationally at the aqueous liquid−vapor interface. At the free liquid surface, the number of H-bonds donated by each water molecule slightly exceeds, on average, the number of H-bonds it accepts at $0.5 < Z < 3$ Å (Figure 4a), and the opposite is true for $Z < 0.5$ Å. This H-bonding configuration results in a net deficiency of donated H-bonds on the vapor side of the interface and a net excess of donating H-bonds on the liquid side. This difference results, on average, in a higher capacity to donate H-bonds than to accept them on the vapor side of the interface and a comparable excess capacity to accept H-bonds on the liquid side. This asymmetry effectively creates a pseudo electric double layer across the interface with a positive field on the vapor side of the interface and a negative field on the liquid side. This electric field structure has long been observed in computer simulations.[14] The pseudo electric double layer should be distinguished from the electric double layer concept that is often used to describe the interfacial separation of ions with different charges, because it is intrinsic to pure water−vapor interfaces and does not require ions to be present. If the local H-bonding imbalance at the water−vapor interface is satisfied by ions in the solution, the cations would be more likely concentrated on the liquid side of the interface (coordinated to the accepting O_{H_2O} ends of the H_2O molecules), and the anions would be concentrated on the vapor side (predominantly coordinated to the donating H_{H_2O} ends of the H_2O molecules). Adsorption of ions may enhance such a double layer.[102] Indeed, the calculated charge density profile of water at the water−vapor interface shows clearly that positive charge density on the vapor side of the interface and negative charge density on the liquid side (Figure 5a). It is also interesting to observe that the Gibbs dividing surface occurs close to the boundary between positive and negative regions of charge density.

At the water−talc interface, the number of donated H-bonds exceeds the number of accepted H-bonds at $Z < 3$ Å (where the water molecules form the first layer at the surface Figures 4b and 1b), but there is no region with a deficiency of donated H-bonds. This difference reflects the molecular scale structure of the talc (001) surface, which is terminated by bridging O_b atoms of the Si−O−Si linkages that are potential weak H-bond acceptors. If the assumption above that a deficiency of accepted H-bonds creates a negative local electric field, which attracts cations from the solution, holds at the talc−water interface, the results here predict that this interface should prefer to adsorb cations. This conclusion is consistent with the charge density profile of water at talc (001) surface. As shown in Figure 5b, a region of negative charge at about $Z = 1.2$ Å is nearly twice as strong as the positively charged regions near $Z = 0.5$ and 3 Å. The high negative charge density attracts positively charged species. Thus, if a talc (001) surface is in contact with an ionic solution, cations would be preferably concentrated at the surface, even though this surface is nominally electrostatically neutral.

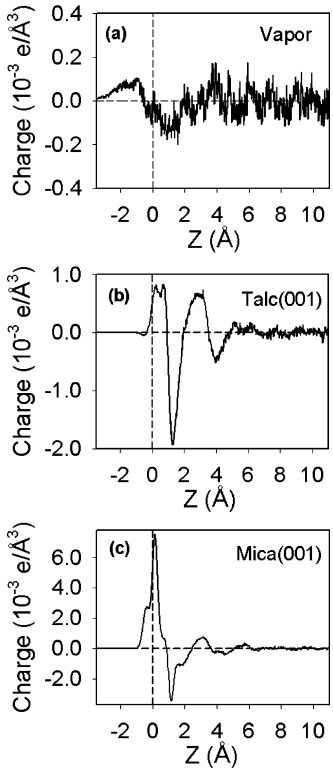

Figure 5. Charge density profiles of water at (a) water−vapor, (b) talc (001), (c) mica (001) interfaces. $Z = 0$ is defined as the position at the Gibbs dividing surface, indicated as dashed vertical line. The horizontal lines indicate zero of average charge density.

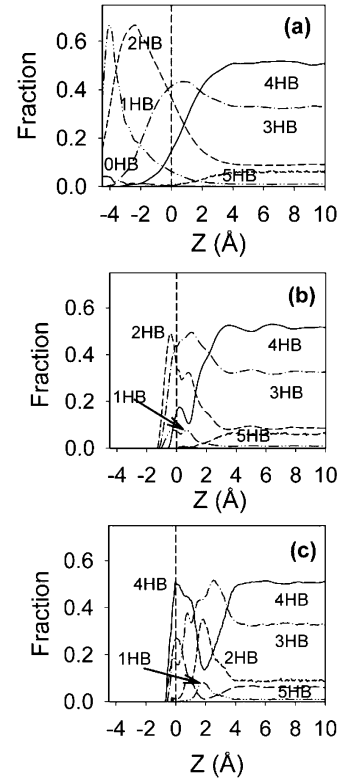

Figure 6. Fraction of water molecules with a certain number of H-bonds as a function of the distance from the surface. (a) At liquid−vapor interface; (b) at talc (001) surface; and (c) at mica (001) surface. Short dashed lines are 5 H-bonded, solid lines are 4 H-bonded, dot-dashed lines are 3 H-bonded, medium dashed lines are 2 H-bonded, dot-dot-dashed lines are 1 H-bonded, and long dashed lines are 0 H-bonded water molecules (monomers). Vertical dashed lines are the Gibbs dividing surface.

In contrast, for the mica−water interface, the number of accepted H-bonds exceeds the number of donated H-bonds at $Z < 4$ Å (Figure 4c) and the charge density at the interface near $Z = 0.2$ Å is positive and more than twice as strong as in negative regions. Therefore, anions are expected to be concentrated locally at distances around $Z = 0.2$ Å from the mica−water interface. The presence of K^+ ions at the mica−water interface, which balance the net structural charge of mica, plays an important role in controlling both the asymmetric H-bonding and the charge density distribution. The positive charge of K^+ ions significantly contributes to the large positive charge density at $Z = 0.2$ Å of the surface. The K^+ ions, which occupy the surface vacancies at $Z \sim 0.2$ Å (Figure 1c), also eliminate the possibility of interfacial water molecules at $Z \sim 2$ Å to donate H-bonds to the surface oxygens (O_b),[51] resulting in the deficit of the donating H-bonds at $Z \sim 2$ Å as shown in Figure 4c.

These specific interactions of ions with the interfaces are caused by the differing abilities of H_2O molecules to form different (donated or accepted) H-bonds with the surfaces. If these predictions are confirmed by future theoretical calculations and experiments, they would have important implications for the interfacial chemical activity of ionic solutions in contact with solid hydrophobic and hydrophobic surfaces. Recent MD simulations of the interface between air and alkali halide solutions[39,40] and experimental second harmonic generation vibrational spectroscopic measurements for the interface between air and aqueous sodium azide and sodium thiocyanide solutions[8,25] show that most anions are preferentially concentrated on the vapor side of the interface. This preference for anions is usually explained by the fact that the anions, especially large ones, are polarized more easily at the interface than the cations.[8,9,102] This explanation does not explicitly take into account the intrinsic electric double layer nature of the interface. Further investigations are required to resolve whether the asymmetric H-bond configuration causes such charge separation or the charge separation is another manifestation of the surface effect.

Spatial Distribution of H-Bonding Environments. The local environments of H_2O molecules at interfaces can be described by the spatial distributions of H_2O molecules having a specific number of H-bonds (Figure 6). Qualitatively, the distributions for the water−vapor, water−talc, and water−mica interfaces are similar with the fraction of H_2O molecules having less than 4 H-bonds increasing toward the interface as the total number of H-bonds decreases (Figure 4). For the mica−water interface, the fraction of water molecules with fewer than 4 H-bonds decreases from the bulk to about $Z = 2$ Å. At $Z < 0$ Å, the fractions of molecules with 0, 1, and 2 H-bonds are noticeably larger for the water−vapor surface, whereas those with 4 and 5 H-bonds are larger for the talc and especially the mica surfaces. These distributions reflect some weak H-bonding at the talc surface and strong H-bonding at the mica surface. At the vapor−liquid interface, the spatial distributions of water molecules with different total numbers of H-bonds have single maxima and can be statistically interpreted as forming layers of predominately *n*-bonded water molecules at different distances (Figure 6a). At the talc−water interface, the distributions are more complex and the peaks are generally narrower (Figure 6b). At the free liquid surface, the water molecules with 0 H-bonds (monomers) occur in the very low density region at $Z < -2$ Å, which may indicate a transition to the vapor phase. At the talc and mica surfaces, the fractions of molecules with 0 H-bonds are negligible, and the fractions with 1 H-bond are small. For talc, most of those 1-bonded molecules occur within

1 Å of the Gibbs dividing plane, and for muscovite they occur near $Z = 2$ Å. Both of these positions are in relatively low density regions.

These MD-computed H-bonding results are consistent with previous experimental sum-frequency[15,18] and near-edge X-ray absorption fine-structure spectroscopic studies[26] and ab initio MD simulations.[19] These results have shown that at the free liquid water surface, the H-bonding environment is complex, and that H_2O molecules with different H-bonding configurations are present including configurations with 0 and 1 donated H-bonds[15,19] and with only accepted H-bonds.[19,26] Our results show that molecules with 0 and 1 H-bonds are present throughout the interface at $Z < 2$ Å (Figure 6a), and that those in acceptor-only configuration become more pronounced at $Z < -3.0$ Å, where the fractions of molecules with 0 and 1 H-bonds are dominant (Figure 6a). A small number of monomers (H_2O molecules with 0 H-bonds) are occasionally present at the free water surface. Remarkably, at $Z \sim 5$ Å, well before the O_{H_2O} density reaches the bulk value (Figure 1), all three interfaces have a very similar distributions of *n*-bonded H_2O molecules (Figure 6). These results thus predict that the H-bonding in this region is not dependent on the structural and compositional details of the surface and that this distance represents an essential H-bonding transition region between the interfacial and bulk liquid water.

Acknowledgment. This research was supported by the DOE BES Geoscience Program (Grants DE-FG02-00ER-15028 and DE-FG02-08ER-15929), and the NSF Center of Advanced Materials for Water Purification with Systems (WaterCAMPWS) at the University of Illinois. The computations were partially supported by the National Center for Supercomputing Applications (Grants EAR000002, TG-EAR990003N) and utilized NCSA hardware and software resources.

References and Notes

(1) Thiel, P. A.; Madey, T. E. *Surf. Sci. Rep.* **1987**, *7*, 211–385.
(2) Hochella, M. F.; White, A. F. *Rev. Mineral.* **1990**, *23*, 1–16.
(3) Robinson, G. W.; Zhu, S.-B.; Singh, S.; Evans, M. W. *Water in biology, chemistry and physics. Experimental overviews and computational methodologies*; World Scientific Publishing Co. Pte. Ltd.: Singapore, 1996; Vol. 9.
(4) Brown, G. E. *Science* **2001**, *294*, 67–70.
(5) Henderson, M. A. *Surf. Sci. Rep.* **2002**, *46*, 1–308.
(6) Pratt, L. R.; Pohorille, A. *Chem. Rev.* **2002**, *102*, 2671–2692.
(7) Bagchi, B. *Chem. Rev.* **2005**, *105*, 3197–3219.
(8) Petersen, P. B.; Saykally, R. J. *Annu. Rev. Phys. Chem.* **2006**, *57*, 333–364.
(9) Jungwirth, P.; Tobias, D. J. *Chem. Rev.* **2006**, *106*, 1259–1281.
(10) Stillinger, F. H. *J. Solution Chem.* **1973**, *2*, 141–158.
(11) Chandler, D. *Nature* **2005**, *437*, 640–647.
(12) Knipping, E. M.; Lakin, M. J.; Foster, K. L.; Jungwirth, P.; Tobias, D. J.; Gerber, R. B.; Dabdub, D.; Finlayson-Pitts, B. J. *Science* **2000**, *288*, 301–306.
(13) Jungwirth, P.; Tobias, D. J. *J. Phys. Chem. B* **2001**, *105*, 10468–10472.
(14) Wilson, M. A.; Pohorille, A.; Pratt, L. R. *J. Phys. Chem.* **1987**, *91*, 4873–4878.
(15) Du, Q.; Superfine, R.; Freysz, E.; Shen, Y. R. *Phys. Rev. Lett.* **1993**, *70*, 2313.
(16) Du, Q.; Freysz, E.; Shen, Y. R. *Science* **1994**, *264*, 826–828.
(17) Alejandre, J.; Tildesley, D. J.; Chapela, G. A. *J. Chem. Phys.* **1995**, *102*, 4574–4583.
(18) Scatena, L. F.; Brown, M. G.; Richmond, G. L. *Science* **2001**, *292*, 908–912.
(19) Kuo, I.-F. W.; Mundy, C. J. *Science* **2004**, *303*, 658–660.
(20) Bresme, F.; Chacon, E.; Tarazona, P.; Tay, K. *Phys. Rev. Lett.* **2008**, *101*, 056102–056104.
(21) Ji, N.; Ostroverkhov, V.; Tian, C. S.; Shen, Y. R. *Phys. Rev. Lett.* **2008**, *100*, 096102–096104.
(22) Abraham, F. F. *J. Chem. Phys.* **1978**, *68*, 3713–3716.
(23) Yu, C.-J.; Richter, A. G.; Datta, A.; Durbin, M. K.; Dutta, P. *Phys. Rev. Lett.* **1999**, *82*, 2326–2329.
(24) Petersen, P. B.; Saykally, R. J. *Chem. Phys. Lett.* **2004**, *397*, 51–55.
(25) Petersen, P. B.; Saykally, R. J.; Mucha, M.; Jungwirth, P. *J. Phys. Chem. B* **2005**, *109*, 10915–10921.
(26) Wilson, K. R.; Cavalleri, M.; Rude, B. S.; Schaller, R. D.; Nilsson, A.; Pettersson, L. G. M.; Goldman, N.; Catalano, T.; Bozek, J. D.; Saykally, R. J. *J. Phys.: Condens. Matter* **2002**, *14*, L221.
(27) Soper, A. K. *Mol. Phys.* **2001**, *99*, 1503–1516.
(28) Botti, A.; Bruni, F.; Imberti, S.; Ricci, M. A.; Soper, A. K. *J. Chem. Phys.* **2004**, *121*, 7840–7848.
(29) Smith, J. D.; Cappa, C. D.; Wilson, K. R.; Messer, B. M.; Cohen, R. C.; Saykally, R. J. *Science* **2004**, *306*, 851–853.
(30) Wernet, P.; Nordlund, D.; Bergmann, U.; Cavalleri, M.; Odelius, M.; Ogasawara, H.; Näslund, L. Å.; Hirsch, T. K.; Ojamäe, L.; Glatzel, P.; Pettersson, L. G. M.; Nilsson, A. *Science* **2004**, *304*, 995–999.
(31) Woods, K. N.; Wiedemann, H. *Chem. Phys. Lett.* **2004**, *393*, 159–165.
(32) Fecko, C. J.; Loparo, J. J.; Roberts, S. T.; Tokmakoff, A. *J. Chem. Phys.* **2005**, *122*, 054506.
(33) Imberti, S.; Botti, A.; Bruni, F.; Cappa, G.; Ricci, M. A.; Soper, A. K. *J. Chem. Phys.* **2005**, *122*, 194509.
(34) Mantz, Y. A.; Chen, B.; Martyna, G. J. *Chem. Phys. Lett.* **2005**, *405*, 294–299.
(35) Shen, Y. R.; Ostroverkhov, V. *Chem. Rev.* **2006**, *106*, 1140–1154.
(36) Chacon, E.; Tarazona, P.; Alejandre, J. *J. Chem. Phys.* **2006**, *125*, 014709–014710.
(37) Vassilev, P.; Hartnig, C.; Koper, M. T. M.; Frechard, F.; Santen, R. A. v. *J. Chem. Phys.* **2001**, *115*, 9815–9820.
(38) Dang, L. X.; Chang, T. M. *J. Phys. Chem. B* **2002**, *106*, 235–238.
(39) Garrett, B. C. *Science* **2004**, *303*, 1146–1147.
(40) Jungwirth, P.; Tobias, D. J. *J. Phys. Chem. B* **2002**, *106*, 6361–6373.
(41) Huang, D. M.; Chandler, D. *J. Phys. Chem. B* **2002**, *106*, 2047–2053.
(42) Janecek, J.; Netz, R. R. *Langmuir* **2007**, *23*, 8417–8429.
(43) Jensen, T. R.; Jensen, M. O.; Reitzel, N.; Balashev, K.; Peters, G. H.; Kjaer, K.; Bjornholm, T. *Phys. Rev. Lett.* **2003**, *90*, 086101–086104.
(44) Schwendel, D.; Hayashi, T.; Dahint, R.; Pertsin, A.; Grunze, M.; Steitz, R.; Schreiber, F. *Langmuir* **2003**, *19*, 2284–2293.
(45) Steitz, R.; Gutberlet, T.; Hauss, T.; Klösgen, B.; Krastev, R.; Schemmel, S.; Simonsen, A. C.; Findenegg, G. H. *Langmuir* **2003**, *19*, 2409–2418.
(46) Poynor, A.; Hong, L.; Robinson, I. K.; Granick, S.; Zhang, Z.; Fenter, P. A. *Phys. Rev. Lett.* **2006**, *97*, 266101–266104.
(47) Maccarini, M.; Steitz, R.; Himmelhaus, M.; Fick, J.; Tatur, S.; Wolff, M.; Grunze, M.; Janecek, J.; Netz, R. R. *Langmuir* **2007**, *23*, 598–608.
(48) Kashimoto, K.; Yoon, J.; Hou, B.; Chen, C.-H.; Lin, B.; Aratono, M.; Takiue, T.; Schlossman, M. L. *Phys. Rev. Lett.* **2008**, *101*, 076102–076104.
(49) Wang, J.; Kalinichev, A. G.; Kirkpatrick, R. J. *Geochim. Cosmochim. Acta* **2006**, *70*, 562–582.
(50) Douillard, J. M.; Zajac, J.; Malandrini, H.; Clauss, F. *J. Colloid Interface Sci.* **2002**, *255*, 341–351.
(51) Wang, J.; Kalinichev, A. G.; Kirkpatrick, R. J.; Cygan, R. T. *J. Phys. Chem. B* **2005**, *109*, 15893–15905.
(52) Wang, J.; Kalinichev, A. G.; Kirkpatrick, R. J. *Earth Planet. Sci. Lett.* **2004**, *222*, 517–527.
(53) Wang, J.; Kalinichev, A. G.; Kirkpatrick, R. J. *J. Phys. Chem. B* **2005**, *109*, 14308–14313.
(54) Rayner, J. H.; Brown, G. *Clays Clay Miner.* **1973**, *21*, 103–114.
(55) McKeown, D. A.; Bell, M. I.; Etz, E. S. *Am. Mineral.* **1999**, *84*, 1041–1048.
(56) Cygan, R. T.; Liang, J.-J.; Kalinichev, A. G. *J. Phys. Chem. B* **2004**, *108*, 1255–1266.
(57) Kalinichev, A. G.; Kirkpatrick, R. J.; Cygan, R. T. *Am. Mineral.* **2000**, *85*, 1046–1052.
(58) Wang, J. W.; Kalinichev, A. G.; Kirkpatrick, R. J.; Hou, X. Q. *Chem. Mater.* **2001**, *13*, 145–150.
(59) Kalinichev, A. G.; Kirkpatrick, R. J. *Chem. Mater.* **2002**, *14*, 3539–3549.
(60) Wang, J.; Kalinichev, A. G.; Amonette, J. E.; Kirkpatrick, R. J. *Am. Mineral.* **2003**, *88*, 398–409.
(61) Greathouse, J. A.; Cygan, R. T. *Phys. Chem. Chem. Phys.* **2005**, *7*, 3580–3586.
(62) Kalinichev, A. G.; Wang, J. W.; Kirkpatrick, R. J. *Cem. Concr. Res.* **2007**, *37*, 337–347.
(63) Wang, J.; Rustad, J. R.; Casey, W. H. *Inorg. Chem.* **2007**, *46*, 2962–2964.

(64) Cygan, R. T.; Greathouse, J. A.; Heinz, H.; Kalinichev, A. G. *J. Mater. Chem.* **2009**, *19*, 2470–2481.
(65) Wang, J.; Becker, U. *Am. Mineral.* **2009**, *94*, 380–386.
(66) Teleman, O.; Jönsson, B.; Engström, S. *Mol. Phys.* **1987**, *60*, 193–203.
(67) Berendsen, H. J. C.; Postma, J. P. M.; van Gunsteren, W. F.; Hermans, J. In *Intermolecular Forces*; Pullman, B., Ed.; Riedel: Dordrecht, 1981; pp 331−342.
(68) Guillot, B. *J. Mol. Liq.* **2002**, *101*, 219–260.
(69) Kirkpatrick, R. J.; Kalinichev, A. G.; Wang, J. W. *Mineral. Mag.* **2005**, *69*, 289–308.
(70) Allen, M. P.; Tildesley, D. J. *Computer simulation of liquids*; Clarendon Press: Oxford; 1987.
(71) Kirkpatrick, R. J.; Kalinichev, A. G.; Wang, J. W.; Hou, X. Q.; Amonette, J. E. Molecular modeling of the vibrational spectra of interlayer and surface species of layered double hydroxides. In *Application of Vibrational Spectroscopy to Clay Minerals and Layered Double Hydroxides*; The Clay Mineral Society: Aurora, CO, 2005; Vol. 13, pp 239−285.
(72) Luzar, A. *J. Chem. Phys.* **2000**, *113*, 10663–10675.
(73) Teixeira, J.; Bellissent-Funelt, M.-C.; Chen, S.-H. *J. Phys: Condens. Matter* **1990**, *2*, SA105–SA108.
(74) Aguilella, V. M.; Pellicer, J.; Aguilella-Arzo, M. *Langmuir* **1999**, *15*, 6156–6162.
(75) DeHoff, R. T. *Thermodynamics in Materials Science*; McGraw-Hill: New York, 1993.
(76) Sokhan, V. P.; Tildesley, D. J. *Mol. Phys.* **1997**, *92*, 625–640.
(77) Wagner, W.; Pruss, A. *J. Phys. Chem. Ref. Data* **2002**, *31*, 387–535.
(78) Lee, C.-Y.; McCammon, J. A.; Rossky, P. J. *J. Chem. Phys.* **1984**, *80*, 4448–4455.
(79) Mamatkulov, S. I.; Khabibullaev, P. K.; Netz, R. R. *Langmuir* **2004**, *20*, 4756–4763.
(80) Cheng, L.; Fenter, P.; Nagy, K. L.; Schlegel, M. L.; Sturchio, N. C. *Phys. Rev. Lett.* **2001**, *87*, 156103–156104.
(81) Park, S. H.; Sposito, G. *Phys. Rev. Lett.* **2002**, *89*, 085501–085503.
(82) Meleshyn, A. *J. Phys. Chem. C* **2008**, *112*, 14495–14500.
(83) Argyris, D.; Tummala, N. R.; Striolo, A.; Cole, D. R. *J. Phys. Chem. C* **2008**, *112*, 13587.
(84) Mamontov, E.; Vlcek, L.; Wesolowski, D. J.; Cummings, P. T.; Wang, W.; Anovitz, L. M.; Rosenqvist, J.; Brown, C. M.; Garcia Sakai, V. *J. Phys. Chem. C* **2007**, *111*, 4328.
(85) Bopp, P. A.; Heinzinger, K. *J. Electroanal. Chem.* **1998**, *450*, 165–173.
(86) Dimitrov, D. I.; Raev, N. D.; Semerdzhiev, K. I. *Phys. Chem. Chem. Phys.* **2001**, *3*, 448–452.
(87) Striolo, A.; Chialvo, A. A.; Cummings, P. T.; Gubbins, K. E. *Langmuir* **2003**, *19*, 8583.
(88) Pertsin, A.; Grunze, M. *J. Phys. Chem. B* **2004**, *108*, 1357.
(89) Hirunsit, P.; Balbuena, P. B. *J. Phys. Chem. C* **2007**, *111*, 1709.
(90) Gordillo, M. C.; Marti, J. *Phys. Rev. B* **2008**, *78*, 075432–075435.
(91) Lum, K.; Chandler, D.; Weeks, J. D. *J. Phys. Chem. B* **1999**, *103*, 4570–4577.
(92) Maccarini, M. *Biointerphases* **2007**, *2*, MR1–MR15.
(93) Ocko, B. M.; Dhinojwala, A.; Daillant, J. *Phys. Rev. Lett.* **2008**, *101*, 039601–039601.
(94) Poynor, A.; Hong, L.; Robinson, I. K.; Granick, S.; Fenter, P. A.; Zhang, Z. *Phys. Rev. Lett.* **2008**, *101*, 039602–039601.
(95) Ohtaki, H.; Radnai, T. *Chem. Rev.* **1993**, *93*, 1157–1204.
(96) Grigera, J. R.; Kalko, S. G.; Fischbarg, J. *Langmuir* **1996**, *12*, 154–158.
(97) Jedlovszky, P.; Vincze, A.; Horvai, G. *J. Chem. Phys.* **2002**, *117*, 2271–2280.
(98) Bridgeman, C. H.; Skipper, N. T. *J. Phys.: Condens. Matter* **1997**, *9*, 4081–4087.
(99) Kalinichev, A. G.; Gorbaty, Y. E.; Okhulkov, A. V. *J. Mol. Liq.* **1999**, *82*, 57–72.
(100) Head-Gordon, T.; Hura, G. *Chem. Rev.* **2002**, *102*, 2651–2669.
(101) Kumar, R.; Schmidt, J. R.; Skinner, J. L. *J. Chem. Phys.* **2007**, *126*, 204107.
(102) Warren, G. L.; Patel, S. *J. Phys. Chem. B* **2008**, *112*, 11679–11693.

JP9018316